Oscillatory magnetic anisotropy and spin-reorientation induced by heavy-metal cap in Cu/FeCo/M (M=Hf or Ta): A first-principles study

P. V. Ong, Nicholas Kioussis, P. Khalili Amiri, and K. L. Wang

Phys. Rev. B **94**, 174404 — Published 3 November 2016

DOI: 10.1103/PhysRevB.94.174404

Oscillatory magnetic anisotropy and spin-reorientation induced by heavy-metal cap in Cu/FeCo/HM (HM=Hf or Ta): A first-principles study

P. V. Ong,[1,*] Nicholas Kioussis,[1,†] P. Khalili Amiri,[2,3] and K. L. Wang[2]

[1] *Department of Physics and Astronomy, California State University Northridge, Northridge, California 91330, USA*
[2] *Department of Electrical Engineering, University of California, Los Angeles, California 90095, USA*
[3] *Inston Inc., Los Angeles, California 90095, USA*

(Dated: October 10, 2016)

Using *ab initio* electronic structure calculations we have investigated the effect of thickness of heavy metal (HM) cap on the magnetic anisotropy of the Cu/FeCo/HM(n) thin film, where HM=Hf and Ta with thickness n=0-10 monolayers (MLs). We find that the Hf cap results in a large perpendicular magnetic anisotropy (PMA), which exhibits quasi-periodic oscillation with a period of 2-MLs. In contrast, the Ta-capped heterostructure exhibits a spin reorientation from out-of to in-plane magnetization orientation at 2-MLs of Ta. Moreover, the MA remains negative and depends weakly on Ta cap thickness beyond the critical thickness. The underlying mechanism of the PMA oscillation is the periodic change of spin-flip spin-orbit coupling (SOC) between the minority-spin Fe $d(xz, yz)$ and majority Fe $d(z^2)$ at $\overline{\Gamma}$, which is induced by the hybridization with Hf at the FeCo/Hf interface. Our results help resolve the contradictory experiments regarding the role of the FeCo/Ta interface on the PMA of the MgO/FeCo/Ta junction. The calculations reveal that the ferromagnet/Hf is promising for spintronic applications and that the capping material and thickness are additional parameters for optimizing the functional properties of spintronic devices.

PACS numbers: 75.30.Gw, 75.70.Cn, 75.85.+t, 73.20.-r

I. INTRODUCTION

Perpendicular magnetic anisotropy (PMA) in trilayers of nonmagnetic metal/ferromagnet/heavy metal (NM/FM/HM) or insulator/ferromagnet/heavy metal (I/FM/HM) is of great interest for spintronic applications such as spin-transfer-torque random access memory (STT-RAM),[1,2] magnetoelectric RAM,[3,4] and spin valves.[5–9] These perpendicularly magnetized heterostructures, where the NM and I layers are usually Cu and MgO, respectively, and the HM layer (Ru, Pd, Hf, Ta, Pt, Au) has strong spin orbit coupling (SOC), promise lower critical current for magnetization switching, faster magnetic switching, smaller magnetic bits, and high thermal stability.[1,9,10] Recently, it was shown that the material type and thickness of the HM layer play crucial role not only on the MA[11–17] but also on the voltage control[18] and magneto-transport behavior[7,14,16,19,20] of these trilayers. In particular, experiments showed that the Hf overlayer enhances the PMA of MgO/$Co_{20}Fe_{60}B_{20}$/Hf and MgO/$Co_{40}Fe_{40}B_{20}$/Hf over that of MgO/$Co_{20}Fe_{60}B_{20}$/W[16] and MgO/$Co_{40}Fe_{40}B_{20}$/Ta,[17] respectively. Similar results have also been predicted from *ab initio* calculations on Fe/Hf and Fe/Ta superlattices, where the thicknesses of each FM and HM layer is 9 monolayers (MLs).[21]

On the other hand, experimental results on the effect of Ta on MA of MgO/CoFeB remain controversial. Worledge *et al.*[22] showed that the magnetization orientation of MgO/$Co_{60}Fe_{20}B_{20}$/Ru remains in-plane for FM thickness down to 0.5 nm while that of MgO/$Co_{60}Fe_{20}B_{20}$/Ta becomes perpendicular at around 0.9 nm, indicating that the CoFeB/Ta interface provides a PMA contribution. A similar conclusion was also drawn from experiments by Liu *et al.*[17] In contrast, Yamamoto *et al.*[13] showed that in MgO (1 nm)/$Co_{20}Fe_{60}B_{20}$/cap the MA decreases when the cap is successively replaced by 5-nm-thick MgO, Ta, and Ru, respectively. Moreover, these experiments reported that there is no PMA in Ta/$Co_{20}Fe_{60}B_{20}$/Ta, indicating that the CoFeB/Ta interface yields negative contribution to the MA. Furthermore, it has been shown that MgO/$Co_{60}Fe_{20}B_{20}$/Ta[14] and MgO/$Co_{20}Fe_{60}B_{20}$/Ta[23] with 1.2-nm-thick FM layer exhibit in-plane magnetization orientation when the Ta thickness exceeds 0.45 nm and 2 nm, respectively.

Besides the Ta thickness, the annealing time and temperature which govern the diffusion of Ta across the interfaces have been shown to have a strong effect on the MA of the MgO/CoFeB/Ta junction.[1,7,24,25] Therefore, given the contradictory results and ill-defined structural characteristics of the I/FM and FM/HM interfaces, current experiments could not provide an unambiguous and consistent interpretation of the role of the FeCoB/Ta interface on the PMA of the magnetic junctions. Furthermore, it is well-known that by varying the thickness of the FM thin film or the HM cap can induce shifts of spin-polarized quantum well states, resulting in strong variation of the MA[26] and even a switching of the magnetic easy axis of thin films.[27] This raises another interesting question when comparing the MA of the Hf- and Ta-capped systems, namely, whether the enhancement of the MA of the FM/Hf over that of FM/Ta interface is specific to certain thickness range of the HM cap or is it generally true.

In this work, we report *ab initio* electronic structure calculations of the effect of the HM cap thickness on the MA in Cu/FeCo/HM (HM= Ta, Hf). Our results show

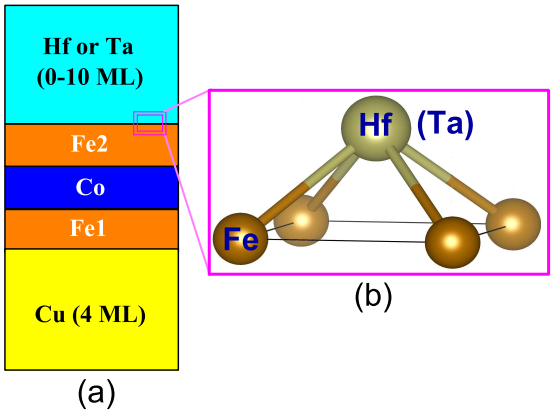

FIG. 1. (Color online) (a) Schematic model of Cu/FeCo/HM(n) trilayer, where HM = Hf or Ta and n=0-10 MLs. (b) Tetragonal pyramidal structure at the FeCo/HM interface.

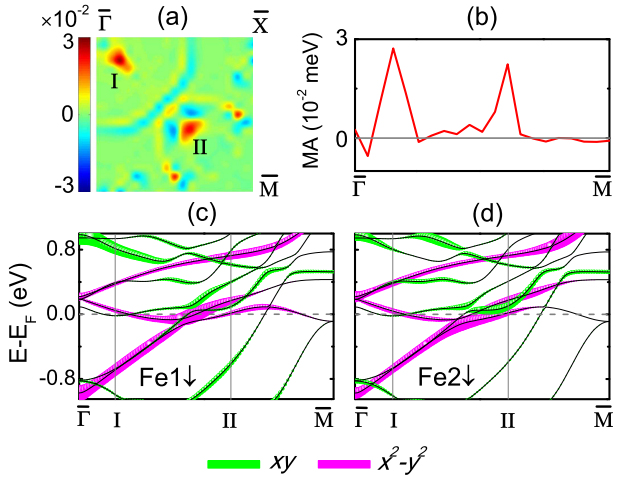

FIG. 2. (Color online) Cu/FeCo/vacuum: (a) and (b) MA(**k**) (in meV) in the 2D BZ and along $\overline{\Gamma M}$, respectively. In (a), I and II indicate the BZ $\mathbf{k}_{\parallel}$ points, where there are large positive contributions to MA. (c) and (d) Energy- and k-resolved distribution of orbital character of minority-spin (↓) bands along $\overline{\Gamma M}$ for the Fe1- and Fe2- derived d_{xy} and $d_{x^2-y^2}$ states, respectively.

distinct differences of the effect of Ta and Hf capping on the MA of the trilayers and resolve the above questions. The underlying mechanism is elucidated by mapping the k-resolved MA and analyzing the energy and k-resolved distributions of the $d-$ states of the minority- and majority-spin bands. The rest of this paper is organized as follows: Sec. II describes the methodology used to calculate the MA. In Sec. III A we consider the limit of zero cap thickness, *i.e.* Cu/FeCo/vacuum and investigate the origin in electronic structure of the PMA in the uncapped system. In Sec. III B, we demonstrate that the PMA of the Cu/FeCo/Hf trilayer oscillates with Hf thickness and elucidate the mechanism of the oscillatory behavior. In Sec. III C, we show that Ta capping induces a spin-reorientation in Cu/FeCo/Ta and discuss the mechanism of the thickness-induced magnetic switching. Finally, conclusions are summarized in Sec. IV.

II. COMPUTATIONAL METHODS AND MODELS

There are different approaches to calculate the MA in magnetic alloys. For example, one approach to calculate the MA and its thermal variation is based on the relativistic extension of the Korringa-Kohn-Rostoker multiple scattering theory within coherent potential approximation (CPA) using the magnetic torque.[28] In this work, the *ab initio* calculations have been carried out within the framework of the projector augmented-wave (PAW) formalism,[29] as implemented in the Vienna *ab initio* simulation package (VASP).[30,31] It has been shown that MA values calculated from the supercell approach within the PAW methodology with SOC are in good agreement with those calculated within the CPA and other full potential methods, and for Fe-Co alloys very well describe experimental data for tetragonally distorted thin films.[32] The generalized gradient approximation[33] is employed to treat the exchange-correlation interaction. For $Fe_{1-x}Co_x$ alloys with $x \sim 0.5$, the MA values calculated at the levels of local density approximation and GGA exhibit no significant difference.[32] Cu/FeCO/Hf(Ta) trilayers are modeled by a slab supercell approach along [001] consisting of four MLs of fcc Cu rotated by 45° on the (001) plane, three MLs of $B2$-type FeCo, zero to ten MLs of Hf or Ta, and a 15Å-thick vacuum separating the periodic slabs (Fig. 1). In experiment, HM caps grow on the FM layer in an amorphous form.[19,34] In the present work, we assume the Hf layer has a fcc or bcc structure. We denote with Fe1 and Fe2 the iron atoms at the Fe/Cu and Fe/Hf(Ta) interfaces, respectively. The in-plane lattice constant is fixed at the calculated value of bulk FeCo lattice constant (2.840Å). The magnetic and electronic degrees of freedom and atomic z positions are relaxed until the forces acting on the ions become less than 2×10^{-3} eV/Å and the change in the total energy between two ionic relaxation steps is smaller than 10^{-6} eV. The plane-wave cutoff energy is 500 eV and the Monkhorst-Pack k-mesh was $17 \times 17 \times 1$ for the relaxations. SOC of the valence electrons is then included using the second-variation method[35] employing the scalar-relativistic eigenfunctions of the valence states and a $41 \times 41 \times 1$ k-point mesh. The MA per unit interfacial area, A, is determined from MA=$[E_{[100]} - E_{[001]}]/A$, where $E_{[100]}$ and $E_{[001]}$ are the total energies with magnetization along the [100] and [001] directions, respectively. Test calculations with $51 \times 51 \times 1$ k-mesh indicate that the calculated MA values are converged within 10%. For comparison, we also employ the force theorem[36] to calculate the MA $\approx \sum_{\mathbf{k}} \mathrm{MA}(\mathbf{k})/A$, where the k-resolved MA $\mathrm{MA}(\mathbf{k}) = \sum_{n \in occ} [\varepsilon(n,\mathbf{k})^{[100]} - \varepsilon(n,\mathbf{k})^{[001]}]$ with the band index n running over all occupied (occ) states.

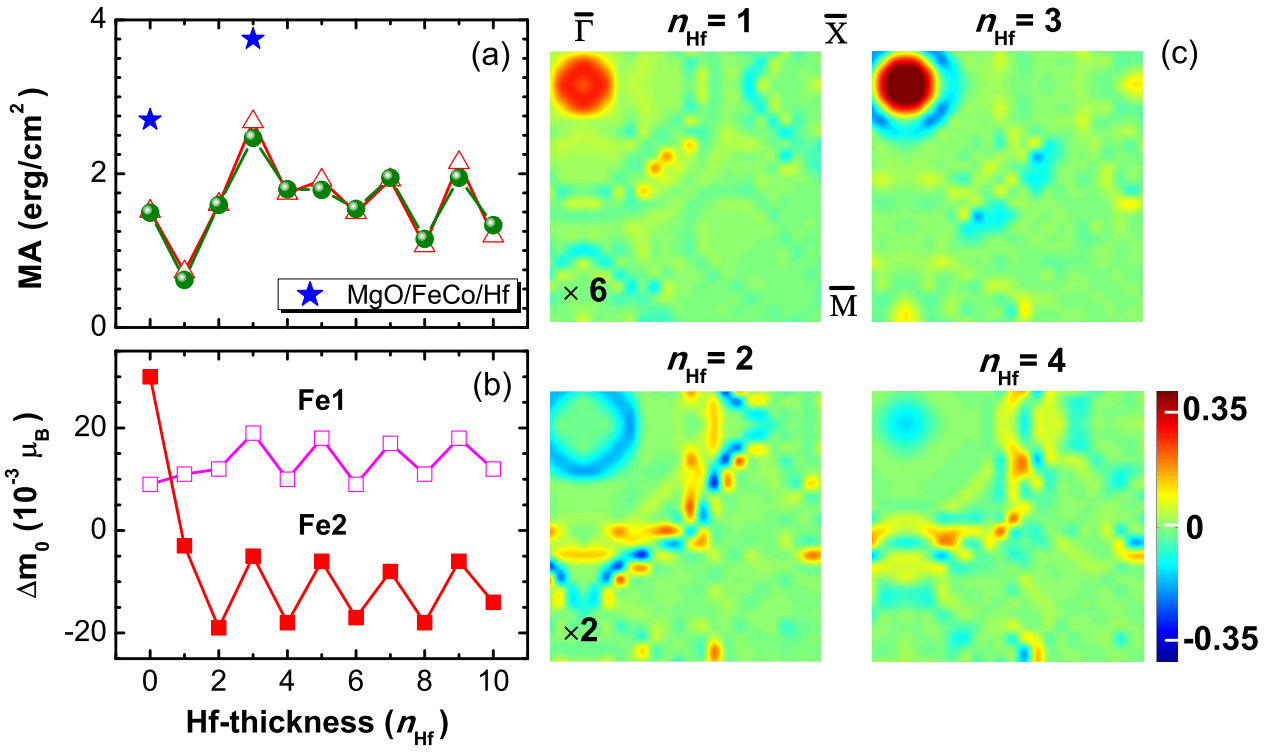

FIG. 3. (Color online) (a) Cap-thickness dependence of MA of Cu/FeCo/Hf, calculated using total energy difference (circles) and the force theorem (triangles). The stars indicate MA of MgO/FeCo/Hf(n) for $n=$ 0 and 3 MLs. (b) Cap-thickness dependence of orbital moment difference, $\Delta m_o = m_o^{[001]} - m_o^{[100]}$, of the Fe1 and Fe2 interfacial atoms. (c) MA($\mathbf{k}$) contours (in meV) in the 2D BZ for Hf thickness $n_{\rm Hf}$=1, 2, 3, 4. For the sake of clarity, MA($\mathbf{k}$) is magnified by factors of 6 and 2 for $n_{\rm Hf}$=1 and 2, respectively.

Here, the sum with respect to $\mathbf{k}$ is taken over the two-dimensional Brillouin zone (2D BZ) and $\varepsilon(n,\mathbf{k})^{[100](\![001]\!])}$ are the eigenvalues of the Hamiltonian for magnetization along the [100] ([001]) direction, respectively.

III. RESULTS AND DISCUSSION

A. Perpendicular magnetic anisotropy of Cu/FeCo/vacuum

Figure 2(a) and (b) show MA($\mathbf{k}$) in 2D BZ and along $\overline{\Gamma\mathrm{M}}$, respectively. We also show in Fig. 2(c) and (d) the energy- and k-resolved distribution of the minority-spin ($\downarrow$) Fe1 and Fe2 d-states, respectively, along $\overline{\Gamma\mathrm{M}}$.

The main PMA contributions occur at BZ points I and II (BZP-I and BZP-II, respectively) along $\overline{\Gamma\mathrm{M}}$ [Fig. 2(a) and (b)]. Within second-order perturbation theory the MA can be expressed as[39]

$$MCA \propto \xi^2 \sum_{\mathbf{k}} \sum_{o,u} \frac{|\langle\Psi^{\downarrow}_{\mathbf{k}o}|\hat{L}_z|\Psi^{\downarrow}_{\mathbf{k}u}\rangle|^2 - |\langle\Psi^{\downarrow}_{\mathbf{k}o}|\hat{L}_x|\Psi^{\downarrow}_{\mathbf{k}u}\rangle|^2}{E^{\downarrow}_{\mathbf{k}u} - E^{\downarrow}_{\mathbf{k}o}},$$

$$+\xi^2 \sum_{\mathbf{k}} \sum_{o,u} \frac{|\langle\Psi^{\uparrow}_{\mathbf{k}o}|\hat{L}_x|\Psi^{\downarrow}_{\mathbf{k}u}\rangle|^2 - |\langle\Psi^{\uparrow}_{\mathbf{k}o}|\hat{L}_z|\Psi^{\downarrow}_{\mathbf{k}u}\rangle|^2}{E^{\downarrow}_{\mathbf{k}u} - E^{\uparrow}_{\mathbf{k}o}}. \quad (1)$$

Here, $\Psi^{\downarrow}_{\mathbf{k}o}$ ($E^{\downarrow}_{\mathbf{k}o}$), $\Psi^{\uparrow}_{\mathbf{k}o}$ ($E^{\uparrow}_{\mathbf{k}o}$), and $\Psi^{\downarrow}_{\mathbf{k}u}$ ($E^{\downarrow}_{\mathbf{k}u}$) are occupied minority, occupied majority, and unoccupied minority-spin states (energies); ξ is the SOC constant and $\hat{L}_{x(z)}$ is the x (z) component of the orbital angular momentum operator. Note that the contribution from the spin-flip SOC term has opposite sign from the SOC term between states of the same spin.

The origin of the positive MA at BZP-I and -II is mainly due to the SOC of occupied Fe1$\downarrow$ $d(x^2-y^2)$ state to unoccupied $d(xy)$ states and that of the occupied Fe1$\downarrow$ $d(xy)$ to the unoccupied $d(x^2-y^2)$, respectively, through $\hat{L}_z$ [Fig. 2(c)]. At BZP-I, there is also SOC of occupied Fe2$\downarrow$ $d(x^2-y^2)$ to unoccupied $d(xy)$, giving positive MA contributions. The separation in energy between the occupied and unoccupied Fe2$\downarrow$ d-states is large and out of the energy window at BZP-II [Fig. 2(d)]. Consequently, the MA contribution of the Fe2 atom at this k-point is not significant.

B. Oscillatory magnetic anisotropy in Cu/FeCo/Hf(n)

Figure 3(a) shows the variation of MA with Hf cap thickness ($n_{\rm Hf}$) in Cu/FeCo/Hf trilayer. The MA determined from (i) total energy calculations (circles) and (ii) the force theorem (triangles) are in excellent agree-

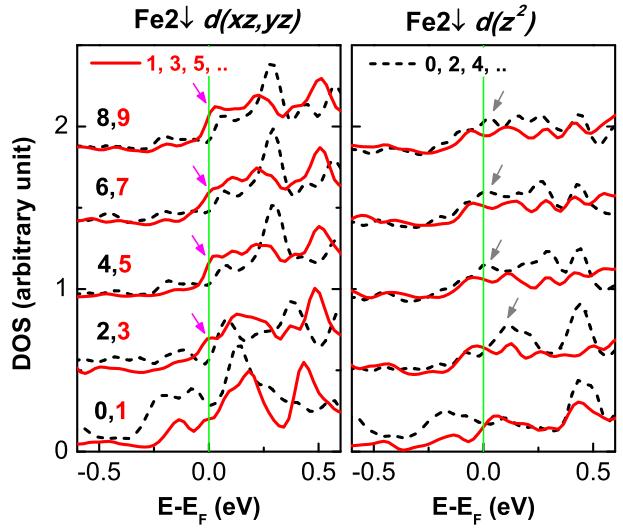

FIG. 4. (Color online) DOS of minority-spin (↓) Fe2-derived $d(xz, yz)$ (left panel) and $d(z^2)$ (right panel) states. Numerals in the left panel indicate Hf thickness $n_{\rm Hf}$= 0-10 MLs. The Fermi level is set to zero energy. The arrows indicate enhancement of $d(xz, yz)$ and $d(z^2)$ DOS which occur periodically near the Fermi level for odd and even $n_{\rm Hf}$, respectively.

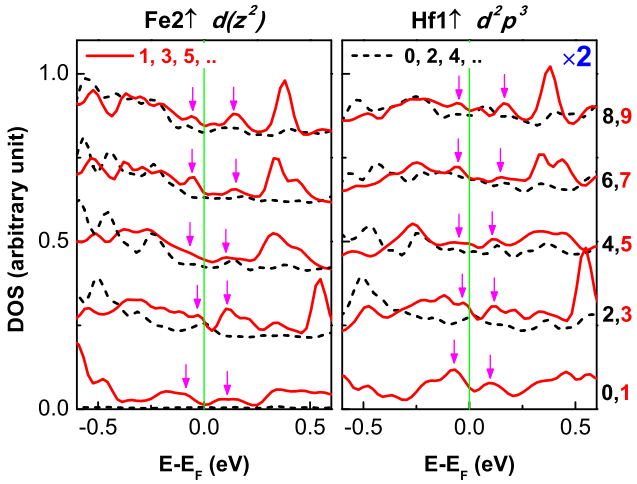

FIG. 5. (Color online) DOS of majority-spin (↑) Fe2-derived $d(z^2)$ states (left panel) and Hf1-derived hybridized d^2p^3=$d(xy)$+$d(z^2)$+$p(x)$+$p(y)$+$p(z)$ states, averaged over the number of the component orbitals (right panel). Numerals on the right panel indicate Hf thickness $n_{\rm Hf}$= 0-10 MLs. The Fermi level is set to zero energy. The arrows indicate enhanced DOS of the $d(z^2)$ or hybridized d^2p^3 states that occur periodically near the Fermi level for odd $n_{\rm Hf}$. For the sake of clarity, the d^2p^3 DOS is magnified by a factor of 2.

ment. For comparison, we also display the MA values of MgO/FeCo/vacuum and MgO/FeCo/Hf(3). The first Hf ML induces a large decrease of MA from 1.49 erg/cm^2 for the Cu/FeCo/vacuum to 0.62 erg/cm^2 for Cu/FeCo/Hf(1). For thin films, the contribution of the shape anisotropy can be estimated by MA_{shape}/t = $-(\mu_0/2)M_S^2$ (SI units),[40,41] where t is the thickness of the FeCo layer and $\mu_0 = 4\pi \times 10^{-7}$ N·A^{-2}. The saturation magnetization is estimated by $M_S = M/V$, where $M = M_{Fe} + M_{Co}$ and V are the total magnetic moment and volume of the unit-cell of the $B2$-type FeCo, respectively. Using $V \sim 23$ Å^3, $M_{Fe} \sim 2.7$ μ_B, and $M_{Co} \sim 1.7$ μ_B, we find $M_S = 1774 \times 10^3$ A·m^{-1}, which is in good agreement with the experimental value of 1950×10^3 A·m^{-1}.[42] Thus, the contribution of the MA_{shape} of about -0.6 erg/cm^2 is smaller than the MA values for the range of Hf thickness considered in this work.

Except for the $n_{\rm Hf} = 1$ ML, the MA values are larger for odd number of Hf layers, resulting in a quasi-periodic oscillation period of 2 MLs, which shows no sign of damping up to 10-ML Hf. The MA($\mathbf{k}$) in 2D BZ is plotted for $n_{\rm Hf}$=1-4 MLs [Fig. 3(c)]. One can clearly see that the enhancement in MA originates from the hot spot at $\overline{\Gamma}$, which appears periodically for odd values of $n_{\rm Hf}$.

We have also calculated the effect of cap-thickness on the orbital moment difference, $\Delta m_o = m_o^{[001]} - m_o^{[100]}$. The results for the interfacial Fe1 and Fe2 atoms are shown in Figure 3(b). For the Co and Hf atoms the variation of Δm_o is much weaker and is not shown. Interestingly, the thickness dependence of Δm_o for Fe1 and Fe2 correlates very well with that of MA and oscillates with the same period of 2 MLs. Note that Δm_o is positive and negative for Fe1 and Fe2, respectively. For single atomic species FM with large exchange splitting, where the spin-flip SOC between states of opposite spins vanishes, Bruno has shown that the MA is proportional to Δm_o.[37] However, for the Cu/FeCo/Hf trilayer the spin-flip term cannot be ignored due to hybridization of Fe2 with the nonmagnetic HM cap. Therefore, the fact that Δm_o is negative for Fe2 does not necessary imply an in-plane magnetic orientation at the FeCo/Hf interface. On the contrary, we show below the FeCo/Hf interface provides a large contribution to PMA, due to the spin-flip SOC induced by hybridization of Fe2 and Hf orbitals.

Figure 4 shows the evolution of density of states (DOS) of the minority-spin Fe2-derived $d(xz, yz)$ and $d(z^2)$ states with Hf thickness. The data clearly shows that the $d(xz, yz)$ DOS around the Fermi level is periodically enhanced for odd values of $n_{\rm Hf}$, except for $n_{\rm Hf} = 1$ ML [left panel in Fig. 4]. On the other hand, the unoccupied $d(z^2)$ DOS is increased for even $n_{\rm Hf}$ [right panel in Fig. 4]. This periodic behavior is consistent with the MA oscillation discussed above. The unoccupied Fe2(↓) $d(z^2)$ and occupied $d(xz, yz)$ are coupled through the $\hat{L}_x$ operator. Therefore, the increase in the unoccupied $d(z^2)$ DOS leads to a decrease in the negative MA term, giving rise to a trough in the MA variation for even $n_{\rm Hf}$.

Figure 5 shows the evolution of DOS of majority-spin Fe2-derived $d(z^2)$ and Hf1-derived hybridized d^2p^3=$d(xy)$+$d(z^2)$+$p(x)$+$p(y)$+$p(z)$ states, averaged over the number of the component orbitals. Since the FeCo/Hf interface has a tetragonal pyramidal structure [Fig. 1(b)], the Hf1-derived hybrid d^2p^3 state is

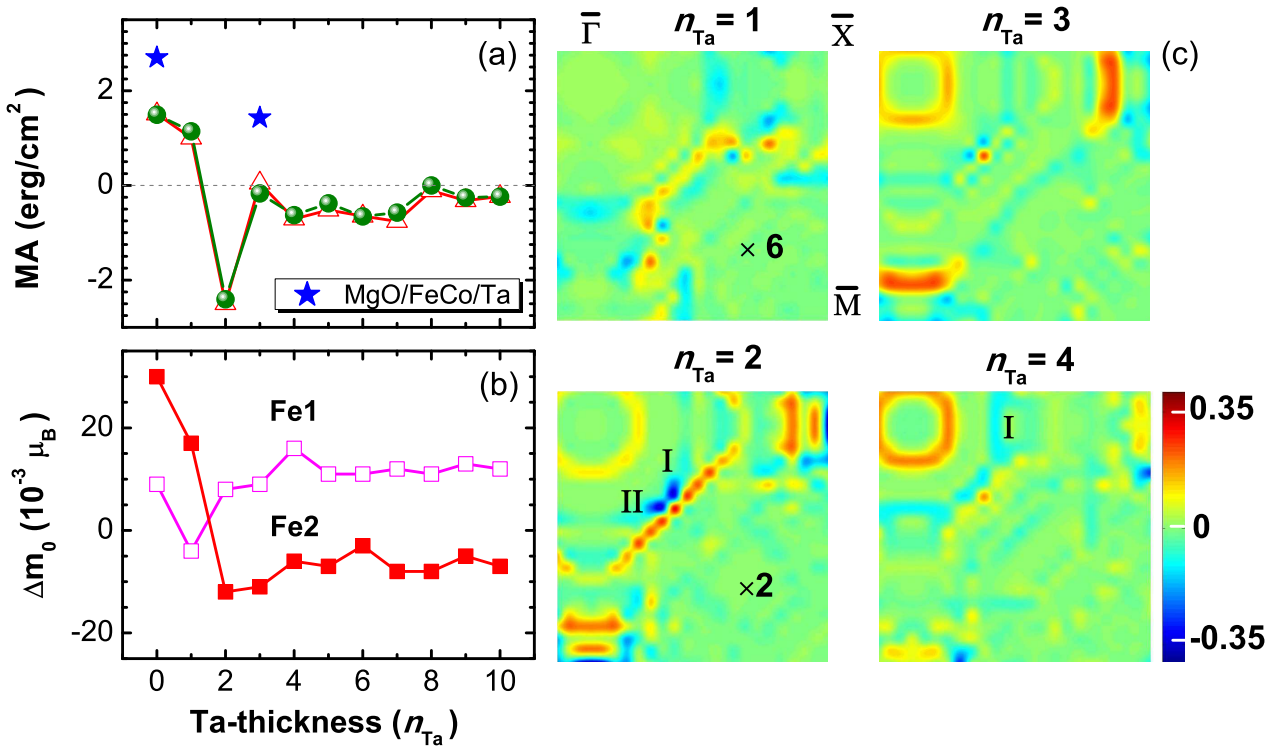

FIG. 6. (Color online) The same as Fig. 3 but for Ta cap. In the MA(**k**) contours for $n_{\rm Ta}$=2 and 4, the points I and II indicate BZP where there are large negative contributions to MA.

allowed.[38]. The consistency in behavior and peak positions of Fe2↑ $d(z^2)$ and Hf1↑ d^2p^3 clearly indicates that there is a strong hybridization between the two orbitals. Note that the DOS of Fe2↑ $d(z^2)$ is enhanced near the Fermi level for odd $n_{\rm Hf}$, in contrast to that of Fe2↓ $d(z^2)$ which increases for even Hf thickness. The calculated energy and k-resolved distribution of orbital characters of majority-spin states shows that the Fe2↑ $d(z^2)$ states occurs exclusively around the $\bar{\Gamma}$ point. The spin-flip SOC between Fe2↑ d_{z^2} and Fe2↓ $d_{xz,yz}$ through $\hat{L}_x$ operator, leads to an enhancement in the positive MA contribution. This gives rise to the MA hot spot in MA(**k**) contours at the $\bar{\Gamma}$ point and explains the peak in MA variation for odd $n_{\rm Hf}$ [Fig. 3(c)].

C. Cap-thickness induced spin-reorientation in Cu/FeCo/Ta(n)

Figure 6(a) shows the variation of MA with Ta cap thickness ($n_{\rm Ta}$) in the Cu/FeCo/Ta trilayer. The MA values calculated using the total energy method and the force theorem are in excellent agreement. In contrast to the oscillatory behavior in the Hf capped system, the MA of Cu/FeCo/Ta(n) abruptly drops to a negative value at $n_{\rm Ta}$ = 2 MLs, leading to a switching of magnetization vector from out-of-plane to in-plane orientation. Using the same method as in Sec. III B, the contribution of the shape anisotropy is calculated to be about −0.6 erg/cm^2, whose absolute value is significantly smaller than the MA at $n_{\rm Ta}$ = 1 (1.0 erg/cm^2). Consequently, the spin-reorientation still persists. For 1 ML-thick Ta cap the MA increases sharply, but remains thereafter negative and exhibits only weak dependence on Ta cap-thickness. For comparison, the MA values of MgO/FeCo/vacuum and MgO/FeCo/Ta(3) are also presented. More specifically, the MA decreases from 2.70 erg/cm^2 for MgO/FeCo/vacuum to 1.43 erg/cm^2 for MgO/FeCo/Ta(3). Note that the MA values of the MgO-supported systems are consistently larger than those of the Cu-supported one. This indicates that the MgO/FeCo induces PMA, while the FeCo/Ta favors in-plane MA. Figure 6(b) shows the orbital moment difference, Δm_o, for the Fe1 and Fe2 atoms versus the thickness of the Ta cap which correlates well with that of the MA. Δm_o rapidly decreases at 1ML and 2 MLs for Fe1 or Fe2, respectively, and thereafter increases and becomes weakly dependent on $n_{\rm Ta}$. The MA(**k**) in 2D BZ is plotted for $n_{\rm Ta}$ = 1–4 MLs [Fig. 6(c)]. In contrast to the MA hot spots found for odd MLs for the Hf cap, we find that the MA vanishes at $\bar{\Gamma}$ for all Ta thicknesses considered in this study.

The electronic configurations of Hf ($5d^2$) and Ta ($5d^3$) differ by one electron. Addition or removal of an electron from the system will lead to an increase or decrease of the Fermi level, respectively. Within the rigid band model, the Fermi-level shift leads to extinction of certain SOC matrix elements and/or establishment of new ones.

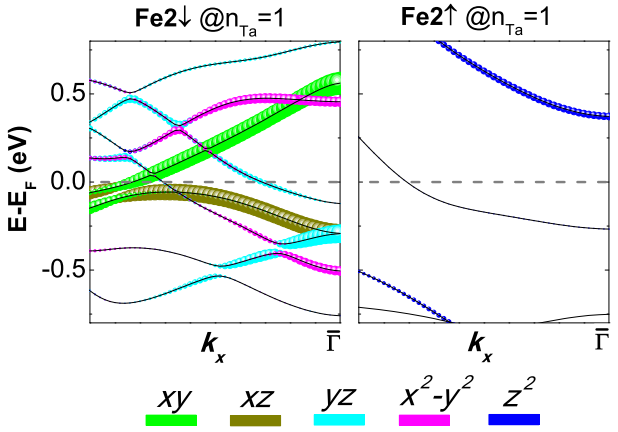

FIG. 7. (Color online) Energy- and k-resolved distribution of orbital character of minority-spin (↓) (left panel) and majority-spin (↑) bands (right panel), respectively, along $\mathbf{k} \parallel \overline{\Gamma X}$ for the interfacial Fe2 atom d-states for $n_{\rm Ta}$=1.

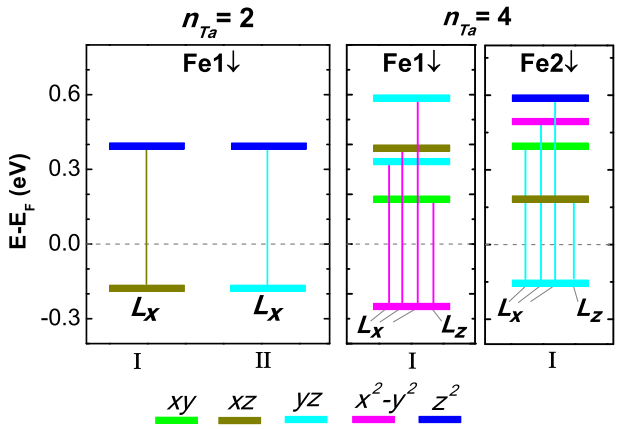

FIG. 8. (Color online) Left panel: energy levels of Fe1-derived minority-spin (↓) states at BZP I and II for $n_{\rm Ta}$=2. Middle and right panels: energy levels of Fe1- and Fe2-derived minority-spin (↓) states, respectively, at the BZP I for $n_{\rm Ta}$=4. Vertical lines connecting pairs of occupied and unoccupied states denote nonvanishing SOC matrix-elements where the line color matches that of the occupied state.

Since the MA energy is determined mainly from spin-orbit-coupled pairs of occupied and unoccupied bands in the vicinity of the Fermi level, these shifts can result in a dramatic change of the MA. Therefore, the distinct behavior of the Hf and Ta capped systems can be understood in terms of the band filling effect.

In order to elucidate the underlying mechanisms of the spin-reorientation and in-plane (negative) MA of the Ta-capped system we have calculated the energy and k-resolved distribution of orbital characters of minority- and majority-spin bands for the Fe1 and Fe2 interfacial atoms for $n_{\rm Ta}$ = 1 which is shown in Fig. 7. The unoccupied Fe2↑ $d(z^2)$ states still occur near the Fermi level at $\overline{\Gamma}$ and they couple to the occupied Fe2↓ $d(xz, yz)$ via spin-flip SOC of $\hat{L}_x$ yielding positive MA contribution. However, this is counterbalanced by the same-spin SOC between the occupied Fe2↓ $d(xz, yz)$ and the unoccupied Fe2↓ $d(xy)$ and $d(x^2 - y^2)$ through $\hat{L}_x$, which yields negative MA contribution. We find similar behavior for thicker Ta cap. The mutual cancelation of MA contributions from the spin-flip and same-spin SOC is responsible for the disappearance of the hot spots at $\overline{\Gamma}$ in MA($\mathbf{k}$) for the Ta-cap trilayers [Fig. 6(c)].

Figure 8 shows the energy levels of the Fe1-derived minority-spin states at the BZP-I and -II for $n_{\rm Ta}$=2 (left panel) and those of Fe1- and Fe2-derived minority-spin states at the BZP-I for $n_{\rm Ta}$=4 (middle and right panels). The associated nonvanishing SOC matrix-elements are represented by vertical lines connecting pairs of occupied and unoccupied states. Because the MA of the Cu/FeCo/Ta system is negative for $n_{\rm Ta}$ = 2 and 4 MLs, we only focus on BZP where MA($\mathbf{k}$) < 0 [Fig. 6(c)]. For $n_{\rm Ta}$=2, the SOC of the occupied Fe1↓ $d(xz)$ with the unoccupied Fe1↓ $d(z^2)$ at point I and that of the occupied Fe1↓ $d(yz)$ with the unoccupied Fe1↓ $d(z^2)$ state at II through $\hat{L}_x$ gives rise to the negative MA($\mathbf{k}$) at BPZ-I and BPZ-II , respectively [left panel in Fig. 8]. For $n_{\rm Ta}$=4, the occupied Fe1↓ $d(x^2 - y^2)$ (middle panel in Fig. 8) is coupled to the unoccupied Fe1↓ $d(xz)$ and $d(yz)$ through $\hat{L}_x$ and to the unoccupied Fe1↓ $d(xy)$ through $\hat{L}_z$. For the Fe2 site the occupied Fe2↓ $d(yz)$ at point I is coupled to the unoccupied Fe2↓ $d(xy)$, $d(x^2 - y^2)$ and $d(z^2)$ through $\hat{L}_x$ and to the unoccupied Fe2↓ $d(xz)$ through $\hat{L}_z$. The competition between the negative and positive MA contributions due to these SOC through $\hat{L}_x$ and $\hat{L}_z$, respectively, renders MA($\mathbf{k}$) < 0 at the BZP-I [right panel in Fig. 8].

IV. CONCLUSION

In summary, using electronic structure calculations we have studied the effects of HM cap on the MA of Cu/FeCo/HM(n) thin film where HM=Hf and Ta with thickness n = 0-10 MLs. We showed that the Hf cap induces large PMA, which exhibits quasi-periodic oscillation with cap thickness. The oscillation has a period of 2-MLs and shows no sign of damping up to 10 MLs of cap thickness. The underlying mechanism of the oscillatory behavior is the periodic change in the spin-flip SOC at $\overline{\Gamma}$ between the minority-spin Fe $d(xz, yz)$ and majority-spin Fe $d(z^2)$, which is induced by the hybridization with Hf at the FeCo/Hf interface. On the contrary, the Ta cap induces a spin reorientation from perpendicular to in-plane direction at Ta thickness of 2 MLs. Moreover, the MA remains negative and exhibits weak thickness dependence for thicker Ta cap. We showed that the effect of spin-flip SOC is suppressed in the Cu/FeCo/Ta trilayers, due to the mutual cancelation of MA contributions from the same-spin SOC at $\overline{\Gamma}$. The results unambiguously indicate that the FeCo/Ta interface favors in-plane MA and help

resolve the contradictory experimental results regarding the role of the FeCo/Ta and FeCo/MgO interfaces on the PMA of MgO/FeCo/Ta junctions. Furthermore, our results imply that magnetic multilayers employing Hf cap have large PMA and hence would be promising for spintronic applications.

ACKNOWLEDGMENTS

This research was supported by NSF Grant No. ERC-Translational Applications of Nanoscale Multiferroic Systems (TANMS)-1160504, by Inston Inc, and by NSF Grant No. DMR-1532249.

* phuongvu.ong@csun.edu
† nick.kioussis@csun.edu

[1] S. Ikeda *et. al*, Nature Mater. 9, **721** (2010).
[2] W.-G. Wang, M. Li, S. Hageman, and C. L. Chien, Nature Mater. **11**, 64 (2012).
[3] T. Maruyama *et. al*, Nature Nanotech. **4**, 158 (2009).
[4] Y. Shiota *et. al*, Nature Mater. **11**, 39 (2012).
[5] S. M. Mohseni, R. K. Dumas, Y. Fang, J. W. Lau, S. R. Sani, J. Persson, and Johan Åkerman, Phys. Rev. B. **84**, 174432 (2011).
[6] J. R. Childress, M. J. Carey, M.-C. Cyrille, K. Carey, N. Smith, J. A. Katine, T. D. Boone, A. A. G. Driskill-Smith, S. Maat, K. Mackay, and C. H. Tsang, IEEE Trans. Magn. **42**, 2444 (2006).
[7] S. Ikeda, J. Hayakawa, Y. Ashizawa, Y. M. Lee, K. Miura, H. Hasegawa, M. Tsunoda, F. Matsukura, and H. Ohno, Appl. Phys. Lett. **93**, 082508 (2008).
[8] H. Kanai, J. Kane, K. Yamada, K. Aoshima, M. Kanamine, J. Toda, and Y. Mizoshita, IEEE Trans. Magn. **33**, 2872 (1997).
[9] S. Mangin, D. Ravelosona, J. A. Katine, M. J. Carey, B. D. Terris, and E. E. Fullerton, Nat. Mater. **5**, 210 (2006).
[10] S. Mangin, Y. Henry, D. Ravelosona, J. A. Katine, and E. E. Fullerton, Appl. Phys. Lett. **94**, 012502 (2009).
[11] D.-Y. Lee, T.-H. Shim, and J.-G. Park, Appl. Phys. Lett. **102**, 212409 (2013).
[12] J. Sinha, M. Hayashi, A. J. Kellock, S. Fukami, M.Yamanouchi, H. Sato, S. Ikeda, S. Mitani, See.-hun Yang, S. S. P. Parkin, and H. Ohno, Appl. Phys. Lett. **102**, 242405 (2013).
[13] H. Yamamoto, J. Hayakawa, K. Miura, K. Ito, H. Matsuoka, S. Ikeda, and H. Ohno, Appl. Phys. Express **5**, 053002 (2012).
[14] L. Cuchet, B. Rodmacq, S. Auffret, R. C. Sousa, C. Ducruet, and B. Dieny, Appl. Phys. Lett. **103**, 052402 (2013).
[15] M. P. R. Sabino, S. T. Lim, and M. Tran, Appl. Phys. Express **7**, 093002 (2014) .
[16] C.-F. Pai, M.-H. Nguyen, C. Belvin, L. H. Vilela-Leão, D. C. Ralph, and R. A. Buhrman, Appl. Phys. Lett. **104**, 082407 (2014).
[17] T. Liu, J. W. Cai, and Li Sun, AIP Advances **2**, 032151 (2012).
[18] Y. Shiota, F. Bonell, S. Miwa, N. Mizuochi, T. Shinjo, and Y. Suzuki, Appl. Phys. Lett. **103**, 082410 (2013).
[19] S. V. Karthik, Y. K. Takahashi, T. Ohkubo, K. Hono, H. D. Gan, S. Ikeda, and H. Ohno, J. Appl. Phys. **111**, 083922 (2012).
[20] P. W. T. Pong and W. F. Egelhoff, J. Appl. Phys. **105**, 07C915 (2009).
[21] Y. Miura, M. Tsujikawa, and M. Shirai, J. Appl. Phys. **113**, 233908 (2013).
[22] D. C. Worledge, G. Hu, D. W. Abraham, J. Z. Sun, P. L. Trouilloud, J. Nowak, S. Brown, M. C. Gaidis, E. J. O'Sullivan, and R. P. Robertazzi, Appl. Phys. Lett. **98**, 022501 (2011).
[23] C.-W. Cheng, W. Feng, G. Chern, C. M. Lee, and T. Wu, J. Appl. Phys. **110**, 033916 (2011).
[24] N. Miyakawa, D. C. Worledge, and K. Kita, IEEE Magn. Lett. **4**, 1000104 (2013).
[25] W.-G. Wang, S. Hageman, M. Li, S. Huang, X. Kou, X. Fan, J. Q. Xiao, and C. L. Chien, Appl. Phys. Lett. **99**, 102502 (2011).
[26] M. Przybylski, M. Dabrowski, U. Bauer, M. Cinal, and J. Kirschner, J. Appl. Phys. **111**, 07C102 (2012).
[27] P. V. Ong, N. Kioussis, P. Khalili Amiri, J. G Alzate, K. L. Wang, G. P. Carman, J. Hu, and R. Wu, Phys. Rev. B **89**, 094422 (2014).
[28] J. B. Staunton, L. Szunyogh, A. Buruzs, B. L. Gyorffy, S. Ostanin, and L. Udvardi, Phys. Rev. B **74**, 144411, (2006).
[29] P. E. Blöchl, Phys. Rev. B **50**, 17953 (1994).
[30] G. Kresse and J. Furthmüller, Phys. Rev. B **54**, 11169 (1996).
[31] G. Kresse and J. Furthmüller , Comput. Mater. Sci. **6**, 15 (1996).
[32] S. Steiner, S. Khmelevskyi, M. Marsmann, and G. Kresse, Phys. Rev. B. **93**, 224425 (2016).
[33] J. P. Perdew *et. al.*, Phys. Rev. B **46**, 6671 (1992).
[34] T. Miyajima, T. Ibusuki, S. Umehara, M. Sato, S. Eguchi, M. Tsukada, and Y. Kataoka, Appl. Phys. Lett. **94**, 122501 (2009).
[35] D. D. Koelling and B. N. Harmon, J. Phys C: Solid State Phys. **10**, 3107 (1977).
[36] M. Weinert, R. E. Watson, and J. W. Davenport, Phys. Rev. B **32**, 2115 (1985).
[37] C. Andersson, B. Sanyal, O. Eriksson *et. al*, Phys. Rev. Lett. **99**, 177207 (2007).
[38] M. Calvin , C. H. Barkelew, J. Am. Chem. Soc. **68**, 2267 (1946).
[39] D.-S Wang, R. Wu, A. J. Freeman, Phys. Rev. B **47**, 14932 (1993).

[40] P. Bruno, *Physical origins and theoretical models of magnetic anisotropy*, in: Ferienkurse des Forschungszentrums Jülich, Jülich, 1993.

[41] The shape anisotropy is caused by demagnetization field, which is a macroscopic concept and determined only for continuum. Consequently, the shape anisotropy is not strictly valid or fails for ultrathin film whose thickness is several atomic layers. Therefore, this is only a rough estimation of the contribution of the shape anisotropy to the trilayer.

[42] L. Sun, Y. Hao, C. L. Chien, and P. C. Searson, IBM J. Res. Dev **49**, 79 (2005).